

Structural and functional brain alterations in a murine model of angiotensin II-induced hypertension

Anja Meissner, Jens Minnerup, Guadalupe Soria, Anna M Planas

Angaben zur Veröffentlichung / Publication details:

Meissner, Anja, Jens Minnerup, Guadalupe Soria, and Anna M Planas. 2016. "Structural and functional brain alterations in a murine model of angiotensin II-induced hypertension." *Journal of Neurochemistry* 140 (3): 509-21.
<https://doi.org/10.1111/jnc.13905>.

Nutzungsbedingungen / Terms of use:

licgercopyright

Dieses Dokument wird unter folgenden Bedingungen zur Verfügung gestellt: / This document is made available under these conditions:

Deutsches Urheberrecht

Weitere Informationen finden Sie unter: / For more information see:

<https://www.uni-augsburg.de/de/organisation/bibliothek/publizieren-zitieren-archivieren/publiz/>



Structural and functional brain alterations in a murine model of Angiotensin II-induced hypertension

Anja Meissner,^{*,†}  Jens Minnerup,[†] Guadalupe Soria^{*} and Anna M Planas^{*,‡}

^{*}*Institut d'Investigacions Biomèdiques August Pi i Sunyer (IDIBAPS), Barcelona, Spain*

[†]*Department of Neurology, University Hospital Münster, Münster, Germany*

[‡]*Departament d'Isquèmia Cerebral i Neurodegeneració, Institut d'Investigacions Biomèdiques de Barcelona (IIBB), Consejo Superior de Investigaciones Científicas (CSIC), Barcelona, Spain*

Abstract

Hypertension is a main risk factor for the development of cerebral small vessel disease (cSVD) – a major contributor to stroke and the most common cause of vascular dementia. Despite the increasing socioeconomic importance arising from cSVD, currently only a few specific treatment strategies with proven efficacy are known. Fundamental to the lack of specific treatments is poor understanding of the disease pathogenesis and a lack of appropriate animal models resembling all symptoms of the human disease. However, chronic hypertensive rat models have been shown to bear similarities to most key features of cSVD. Despite a significantly larger toolbox available for genotypic and phenotypic modifications compared to rats, mouse models of hypertension are unusual when modeling cSVD and associated cognitive impairment experimentally. In the present study, we therefore characterized hypertension-mediated cerebrovascular alterations and

accompanying structural and functional consequences by simultaneously treating adult wild-type mice (C57BL/6N) with Angiotensin II (AngII) and the nitric oxide synthases inhibitor L-NAME for 4 weeks. Hypertension associated to cerebral alterations reminiscent of early-onset cSVD and vascular cognitive impairment when combined with additional AngII bolus injections. Most importantly, preventing the elevation of blood pressure (BP) protected from the development of cSVD symptoms and associated cognitive decline. Our data strongly support the suitability of this particular mouse model of AngII-induced hypertension as an appropriate animal model for early-onset cSVD and hence, vascular cognitive impairment, pathologies commonly preceding vascular dementia.

Keywords: cerebral small vessel disease, endothelial dysfunction, hypertension, microvasculature, mouse model, vascular dementia.

Vascular dementia (VaD) is recognized as the second most prevalent type of dementia after Alzheimer's disease, accounting for 20% of all dementia cases worldwide (Chui 2001). It is described as the complex loss of cognitive function resulting from cardiovascular or circulatory disturbances that injure brain regions associated with memory, cognition, and behavior. Hemorrhagic or ischemic events, white matter or gray matter lesions, and systemic cardiovascular events leading to central hypoperfusion or cerebrovascular disturbances are representative of the diversity of conditions that can cause VaD, and ultimately complicating the study of its underlying mechanisms (Chui 2001; Brown *et al.* 2007; de la Torre 2012). Cerebral small vessel disease (cSVD), a group of pathological processes affecting the small

Address correspondence and reprint requests to Anja Meissner, Institut d'Investigacions Biomèdiques August Pi i Sunyer (IDIBAPS), Rosello 149-153, 08036 Barcelona, Spain. E-mail: anja.meissner@gmail.com

Abbreviations used: AngII, Angiotensin II; BBB, blood–brain barrier; BP_{sys}, systolic blood pressure; cSVD, cerebral small vessel disease; DTI, diffusion tensor imaging; FA, fractional anisotropy; GFAP, glial fibrillary acidic protein; Iba-1, ionized calcium-binding adapter molecule 1; L-NAME, NG-nitro-L-arginine methyl ester; MCP-1, monocyte chemoattractant protein-1; MRI, magnetic resonance imaging; NOR, novel object recognition; PDGFR-b, beta-type platelet-derived growth factor receptor; RI, recognition index; SHR, spontaneously hypertensive rat; SHRSP, spontaneously hypertensive stroke prone rat; TJ, tight junction; TNF α , tumor necrosis factor alpha; VaD, vascular dementia; VCAM-1, vascular cell adhesion molecule-1; VCI, vascular cognitive impairment.

arteries, arterioles, venules, and capillaries of the brain, is not only a major contributor to stroke in humans but also the most prevalent pathological state leading to vascular cognitive impairment and VaD (Huijts *et al.* 2013, 2014; Yamashiro *et al.* 2014; Meissner 2016). Clinical studies estimate the proportion of VaD caused by cSVD in a range between 36% and 67% (Chui 2001). However, despite the burning medical and socioeconomic importance arising from cSVD and associated cognitive problems, specific treatments are currently missing because of poor understanding of disease pathogenesis and the lack of appropriate animal models.

Since VaD and its preceding forms commonly result from several pathophysiological conditions and risk factors that either alone or in combination promote structural and functional alterations in the brain, the perfect animal model that accounts for etiology, symptomatology, treatment, and physiological basis does not exist. Instead, we find a large variety of animal models that try to mimic disease conditions and outcomes as close as possible to human findings. Specifically for cSVD, the most common cause of VaD (Huijts *et al.* 2013, 2014; Yamashiro *et al.* 2014) animal models are generated by either (i) the induction of local and global hypoperfusion, (ii) genetic modifications, or (iii) chronic hypertension (AngII) (Venkat *et al.* 2015; Gooch and Wilcock 2016; Helman and Murphy 2016). Hypoperfusion models generally lack satisfactory reproducibility of human cSVD as they often result in infarcts and vascular remodeling only distributed to distinct vascular regions. Genetic modifications are very controversially discussed as risk factors for VaD (Rohn 2014; Rohn *et al.* 2014) or limited in terms of generalization as they only represent a rare subtype of the disease (Ayata 2010). Hypertension as a major modifiable risk factor for cSVD, and thus for the development of cognitive impairment (Mitnitski *et al.* 2006; Chang-Quan *et al.* 2011; Imamine *et al.* 2011; de la Torre 2012; Chan *et al.* 2013; Iadecola 2014; Meissner 2016), has been mostly studied in spontaneously hypertensive rats (SHR) (Kaiser *et al.* 2014) and spontaneously hypertensive stroke prone rats (SHRSP) (Henning *et al.* 2010; Jalal *et al.* 2012; Lopez-Gil *et al.* 2014) which to date, represent the most popular models to study brain damage resulting from chronic changes in blood pressure (BP).

Relative to Alzheimer's disease, VaD and preceding forms of cognitive impairment, particularly those emanating from cerebrovascular disease, have been fairly understudied with respect to animal models, pathophysiology, and identification of distinct therapeutic targets. Especially, mechanisms linking cardiovascular risk factors like hypertension to cSVD have yet to be fully elucidated. Establishing a mouse model that reproduces important aspects of the blood vessel pathology would aid both in understanding these disorders and in developing effective treatment strategies, and which appears as a suitable model to study mechanistic links between hypertension and cognitive dysfunction. With the

present study, we intended to characterize the consequences of chronically elevated BP on brain structure and function using a murine model of Angiotensin II (AngII)-induced hypertension, and aimed to establish a mouse model that mimics principal features of hypertension-associated early-onset cSVD.

Material and methods

An expanded Methods section is available in the online Data Supplement.

Materials

All chemical reagents and solutions were purchased from Sigma-Aldrich (Madrid, Spain) unless otherwise stated. Commercially available primary antibodies against alpha-smooth muscle actin, vascular endothelial cadherin, CD3, vWF, ionized calcium-binding adapter molecule 1, NeuN, and brain-derived neurotrophic factor (BDNF) (Abcam, Cambridge, UK), glial fibrillary acidic protein (Dako, Hamburg, Germany), occludin (Life Technologies; Madrid, Spain), and beta-tubulin (Merck Millipore, Darmstadt, Germany) were used for western blotting or immunofluorescence. Secondary antibodies Alexa Fluor donkey anti-mouse or anti-rabbit were purchased from Life Technologies, and horseradish peroxidase-conjugated anti-mouse or anti-rabbit IgG were obtained from GE Healthcare (Madrid, Spain). Primers for qPCR were purchased from Life Technology (Madrid, Spain).

Animals

This investigation conforms to the Guide for Care and Use of Laboratory Animals published by the European Union (Directive 2010/63/EU) and with the ARRIVE guidelines. All animal care and experimental protocols were approved by the institutional animal ethics committees at the University of Barcelona (CEEa) and conducted in accordance with European animal protection laws. Commercially available wild-type mice (C57BL/6N) were purchased from Janvier Laboratories (Madrid, Spain). All mice were housed in a conventional housing facility under a standard 12 : 12 h light–dark cycle, and had access to food (standard rodent diet) and water *ad libitum*. Mice with a body weight (BW) ≥ 25 g were housed in groups of five in conventional transparent polycarbonate cages with inner fitting wire lids and filter tops (1500U EURO-STANDARD TYPE IV S).

Hypertension model

Hypertension was induced using AngII-releasing osmotic mini-pumps as described previously (Wakisaka *et al.* 2010). In brief, wild-type male and female mice (16 weeks old, gender equally distributed to all experimental groups, no sex-based differences in BP responses were present) were anesthetized with isoflurane (1.5% at 1.5 L/min oxygen) for subcutaneous implantation of osmotic mini-pumps (Alzet-1004; Charles River, L'Arbresle, France) containing AngII (1000 ng/kg per min at an infusion rate of 11 μ L/h) ($n = 40$), or an equivalent volume of vehicle (saline) ($n = 15$). Concomitantly, NG-nitro-L-arginine methyl ester (L-NAME) (100 mg/kg BW) was administered to hypertensive groups via drinking water (Wakisaka *et al.* 2010; Toth *et al.* 2015). On day 16

post pump implantation, two hypertensive groups ($n = 25$) received an additional daily bolus of AngII (0.5 $\mu\text{g}/\text{kg}$ BW s.c.). One of these two groups ($n = 10$) received an additional anti-hypertensive therapy starting directly after pump implantation: hydralazine (100 mg/kg BW) was administered via drinking water. Systolic BP was measured frequently in conscious mice using tail-cuff plethysmography (LE 5002; Panlab, Cornella, Spain) starting 4 days before pump implantation after an initial training period of 7 days. For training and trial measurements, mice were placed under a heating lamp 20 min prior to the experiments that were carried out in a dark, quiet environment. During training, mice were accustomed to a mouse strainer by allowing them to enter twice daily for 3 days. On the following training days, mice were slowly accustomed to the BP cuff by inflating the pressure cuff that was placed around their tails, and test measurements were performed. For test trials, BP was measured during early morning hours every other day.

Twenty-two and twenty-five days following pump implantation mice were subjected to magnetic resonance imaging (MRI) scans and cognitive testing, respectively. Animals were sacrificed on day 28, and tissue was distributed to the different experimental approaches. Table S1 provides an overview of experimental groups and experimental timeline.

Animals were randomly assigned to the respective experimental groups using the computer software *Research Randomizer* [Research Randomizer (Version 3.0) retrieved from <http://www.randomizer.org/>]. To ensure blinding, behavioral assessment was performed after the animals had received codes that did not reveal the identity of the treatment.

Study design, including sample size calculations and power analysis

In order to obey the rules for animal welfare, we designed experimental groups in a way that minimizes stress for the animals and guarantees maximal information using the lowest group size possible. For *a priori* sample size calculations, we utilized the software G Power (Faul, Erdfelder, Lang, and Buchner, 2007) and compared the level of a continuous variable in two independent groups in a two-tailed unpaired *t*-test with a type I error rate of $\alpha = 0.05$ (5%) and Power of $1 - \beta > 0.8$ (80%) based on preliminary experiments: for a $\approx 35\%$ reduction of recognition index with a 24-h delay interval (0.67 ± 0.19 to 0.40 ± 0.21 ; mean \pm SD) after 4 weeks of AngII-induced hypertension, we calculated a sample size of $n = 10$ with an effect size of $d = 1.35$. For hypertension-mediated anatomical brain changes visualized using MRI techniques between normotensive and hypertensive mice (T2* analysis: 1.3 ± 0.4 for control and 2.1 ± 0.4 for hypertension), a sample size of $n = 6$ ($d = 2$) was calculated; when using histological methods for ventricle volume assessment (3.8 ± 0.6 for control and 4.8 ± 0.6 for hypertension), a sample size of $n = 7$ ($d = 1.67$) was calculated. For the detection of hypertension-induced changes in cerebral TNF α mRNA expression (1 ± 0.4 for control and 1.75 ± 0.4 for hypertension), a sample size of $n = 5$ ($d = 2.14$) was calculated. In order to conduct all planned experiments, a total sample size of $n = 15$ per group was computed after adjusting for a 15% attrition (corrected sample size = sample size/(1 - [% attrition/100])).

Novel object recognition

A novel object recognition (NOR) task was employed to assess non-spatial memory components. Mice were habituated to the testing

arena for 10 min over a period of 3 days. Habituation and object memory testing was conducted as described previously (Meissner *et al.* 2015). On test day, each mouse was exposed to two objects for 10 min. Five minutes or 24 h later, mice were re-exposed to one object from the original test pair and to a novel object. The placement of the new object was counterbalanced between mice for either the left or right side of the cage to address any confounding influences of handedness. In between testing states, the objects and the cage were wiped with Virox5. The movements of the animal were video tracked with the computer software EthoVision XT[®] (Noldus Information Technology, Wageningen, the Netherlands). A delay interval of (i) 5 min was chosen to test short-term retention of object familiarity, which is dependent on rhinal cortical function (Francis *et al.* 2012; Meissner *et al.* 2015). With delay intervals (ii) longer than 15 min, retention becomes dependent on reactivation of memory traces in the hippocampus (Baker and Kim 2002). A recognition index as the main index of retention was calculated by the time spent investigating the novel object relative to the total object investigation [recognition index = $T_{\text{Novel}}/(T_{\text{Novel}} + T_{\text{Familiar}})$].

MRI-based measurement

MRI experiments were conducted on a 7T BioSpec 70/30 horizontal animal scanner (Bruker BioSpin, Ettlingen, Germany), equipped with a 12-cm inner diameter actively shielded gradient system (400 mT/m) using a surface coil for mouse brain as receiver coil. Animals were placed in a supine position in a Plexiglas holder with a nose cone for administering anesthetic gases (2% isoflurane in a mixture of oxygen and N₂O at a ratio of 30 : 70) and fixed by a tooth bar, ear bars, and adhesive tape. Tripilot scans were carried out for accurate positioning of the animal's head in the isocenter of the magnet.

Diffusion tensor imaging (DTI) experiments were performed using an echo planar imaging sequence with TR = 14 500 ms, TE = 30.85 ms, four segments, $b = 1000$, 30 diffusion directions, five B₀ images, FOV = $20 \times 20 \times 14$ mm³, matrix size = $96 \times 96 \times 28$ pixels³, resulting in an isometric spatial resolution of $0.208 \times 0.208 \times 0.5$ mm³, and an acquisition time of 31 min.

Scalar maps, fractional anisotropy, MD, AD, and RD were calculated with Paravision 5.0 software (Bruker Biospin) and converted to NIFTI format with custom-made programs written in Matlab (The MathWorks, Inc., Natick, MA, USA). Regions of interest were manually drawn in different brain regions to obtain the corresponding DTI scalar map values.

In addition, a FLASH-T2* sequence, showing susceptibility effects where iron is accumulated, was acquired in order to reveal possible microbleedings. The field of view was centered over the anterior hippocampal region and the acquisition parameters were TR = 508 ms, TE = 18 ms, FOV = $20 \times 20 \times 4$ mm³, matrix size = $256 \times 256 \times 19$ pixels³, resulting in an isometric spatial resolution of $0.208 \times 0.208 \times 0.5$ mm³, and acquisition time of 48 min. To evaluate both the eventual microbleedings and the altered microvessels, the following post-processing was performed in software AMIRA[®] v5.2 (Mercury Co, Boston, USA). After skull stripping, a median image filter of noise reduction with kernel 5 was applied and subtracted from the initial image. An intensity threshold, with values comprised between the intensity maximum and its fifth part, was applied to the resulting image and the volume occupied by

the selected pixels was compared between groups. This procedure allowed for automatic segmentation of the microbleedings and hypointensities induced by microvessels.

Microglia quantification

Images were taken from ionized calcium-binding adapter molecule 1-labeled coronal brain sections in the anterior, middle, and posterior cortex using a fluorescent microscope (Nikon Eclipse 80i; Nikon GmbH, Düsseldorf, Germany) at a magnification of 20 \times . The Stereo Investigator Software (MicroBrightField, Inc., Williston, VT, USA) was used for digitizing. Microglia morphology was analyzed using ImageJ (1.48v, <http://imagej.nih.gov/ij>) in three images per area and mouse. For quantifying cell size, cell body, and ramifications, the intensity thresholds and size filter were applied by using the adjust threshold and analyze particles functions. To measure the total cell size, the threshold was maintained at the level that is automatically provided by the program, and no size filter was applied. To measure the total cell body size, the threshold was lowered 40 points and a size filter of 150 pixels was applied. Additionally, the number of cell bodies was counted to give the number of microglia in the area of interest. The total size of the dendritic processes (ramifications) was determined by subtracting the cell body size from the cell size. The total cell size, total cell body size, and total size of dendritic processes were corrected for the number of microglia in the sample area to gain the average size, cell body size, and size of ramifications for each microglial cell in the sample. Finally, the cell body to cell size ratio (%) was determined and utilized as a measurement for microglial activation.

BBB integrity

FITC-dextran (70 kDa; Life Technologies, Madrid, Spain) was intravenously injected (via tail vein) into normotensive and hypertensive wild-type mice, allowed to circulate for 30 min before mice were perfused with saline and 4% paraformaldehyde. In coronal brain section (10 μ m thickness), the fraction that extravasated into the parenchyma and the fraction that remained bound to the vessel wall were analyzed using fluorescence microscopy. The detected fluorescence (at 488 nm) was considered a marker of vascular leakage. Additionally, brain sections were incubated with an antibody against albumin (Abcam, Cambridge, UK) and albumin-positive staining in cortex and hippocampus was analyzed using fluorescence microscopy and quantified using ImageJ (1.48v; <http://imagej.nih.gov/ij>) in three images per area and mouse. To determine the total count of albumin-stained particles in the different brain sections, the adjust threshold and analyze particles functions were used. The threshold was maintained at the level that is automatically provided by the program, and no size filter was applied.

Western blotting, qPCR, and histological experiments

Standard biochemical procedures were utilized for experiments involving reverse transcription polymerase chain reaction, quantitative PCR, western blotting, and histological experiments. Methodological details are provided in the online only Data Supplement.

Statistical analysis

All data are expressed as mean \pm SEM, where n is the number of animals. For comparison of multiple independent groups, one-way ANOVA was used, followed by Bonferroni with exact p value

computation as *post hoc* tests. For comparison of two groups, a two-tailed unpaired t -test was used. Differences were considered significant at error probabilities of ≤ 0.05 .

Results

In order to induce hypertension, wild-type mice were subjected to chronic AngII perfusion and concomitant L-NAME treatment for 28 days. Additionally, mice received a daily AngII bolus starting on day 16 post pump implantation. Throughout the manuscript this group will be referred to as AngII ($n = 15$). A second group received the smooth muscle relaxant hydralazine via drinking water starting directly after pump implantation and will be referred to as AngII + hydralazine ($n = 10$). In order to control for the effects of additional AngII bolus injections starting in week three of hypertension, one group of mice was excluded from the additional bolus treatment and will be referred to as AngII-no bolus ($n = 15$; for an overview of experimental groups see Table S1). In all hypertensive groups, chronic AngII and concomitant L-NAME treatment resulted in a profound increase of systolic BP, which was abolished by simultaneous administration of the vasodilator hydralazine (Table 1). All readouts were compared to results obtained from saline control mice ($n = 15$).

Chronic hypertension induces behavioral alterations

AngII was accompanied by a neuropsychological profile commonly described for vascular cognitive impairment, including slowing of motor performance and information processing, impairments in attention, executive function, and memory (Hachinski 2006; Moorhouse and Rockwood 2008). First, we assessed the activity level of all experimental groups using an open-field setup. AngII mice revealed significantly lower activity levels as evident by a shorter total distance travelled (Fig. 1a), a lower proportion of time spent moving (Fig. 1b), and subsequently, a higher rest time compared to control mice and mice treated with hydralazine. This decreased mobility was confirmed in a forced swim test, a test widely accepted for assessing signs of depression or depression-like behavior (Figure S1a and b). However, hypertension was not associated to an impairment of locomotor responses or visual perception (Figure S1c and d), or to increased anxiety (Table S2).

In order to evaluate memory recognition, we assessed the natural preference for novel objects in a NOR task, which evaluates the rodents' ability to recognize a novel object in a neutral environment. We first performed a hippocampus-independent episodic memory task using a delay interval of 5 min. As evidenced by a significantly lower recognition index, AngII mice showed no clear preference for novel or original objects compared to control mice that spent significantly more time exploring the novel object (Fig. 1c). With delay intervals longer than

Table 1 Hemodynamic parameter of the different experimental groups

	BP sys	<i>p</i> value compared to control	HR	<i>p</i> value compared to control
Control	101.6 ± 6.1		498.3 ± 16.1	
AngII (2 weeks)	120.4 ± 4.5 ^a	0.0128	576.4 ± 27.2	0.2824
AngII	151.6 ± 6.7	0.0001	566.4 ± 17.5	0.0107
AngII – no bolus	150.1 ± 5.8	0.0001	578.1 ± 19.4	0.0073
AngII + hydralazine	103.2 ± 11.7 ^a	0.2872	547.1 ± 31.4	0.1136

Systolic blood pressure (BP sys) and heart rate (HR) values obtained from conscious mice using tail-cuff plethysmography. *n* = 15 per group, ^a*p* ≤ 0.05 compared to Angiotensin II (AngII). Values are expressed as mean ± SEM.

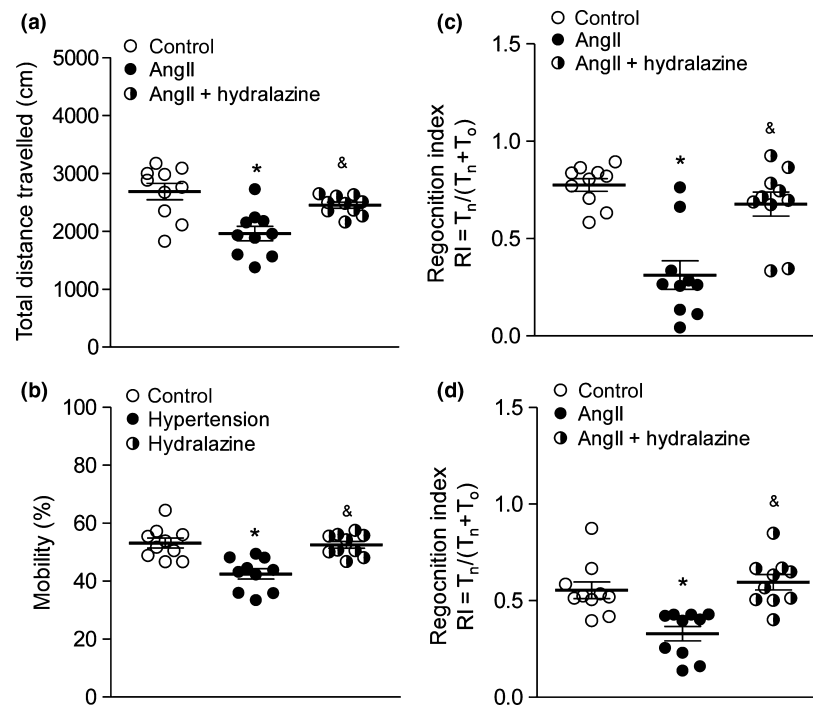


Fig. 1 Hypertension attenuates short- and long-term memory. Locomotor activity was assessed in an open-field task (*n* = 10 per group). Hypertensive mice (a) covered less distance and showed (b) a reduced mobility compared to normotensive and hydralazine-treated mice. (c) Short-term memory function of normotensive, hypertensive mice, and mice receiving hydralazine treatment was determined by a novel object recognition (NOR) task with 5-min delay intervals (*n* = 10 per group). The calculated recognition index (RI) revealed a clear

preference for the familiar rather than the novel object in hypertensive mice. (d) Long-term memory function of normotensive, hypertensive mice, and mice receiving hydralazine treatment was determined by a NOR task with 24-h delay intervals (*n* = 10 per group). The calculated RI revealed a clear preference for the familiar rather than the novel object in hypertensive mice. In (a–d) **p* ≤ 0.05 relative to control and &*p* ≤ 0.05 relative to AngII for multiple, unpaired comparisons.

15 min, retention becomes dependent on reactivation of memory traces in the hippocampus (Baker and Kim 2002; Hammond *et al.* 2004; Francis *et al.* 2012). We therefore performed a second NOR task with a delay interval of 24 h. Again, control animals showed an increase in exploratory behavior when presented with a novel object, while AngII animals failed to differentiate between novel and familiar object (Fig. 1d).

Mice receiving no additional AngII bolus (AngII-no bolus) revealed a lower memory index compared to control mice only when presented to a novel object with a 5 min, but not after a 24-h delay interval (Table 2). Yet, statistical analysis disclosed significant differences to mice that received the additional bolus (AngII) in both test scenarios (*n* = 10 per group, *p* = 0.0494 for 5 min delay and *p* = 0.0141 for 24 h delay). Hydralazine treatment prevented the hypertension-associated

Table 2 Short- and long-term memory function in normotensive and hypertensive mice

	Recognition index 5 min delay	<i>p</i> value compared to control	Recognition index 24 h delay	<i>p</i> value compared to control
Control	0.7691 ± 0.0369		0.5651 ± 0.0535	
AngII (2 weeks)	0.7461 ± 0.0548	0.4027	0.5840 ± 0.0485	0.9706
AngII	0.3183 ± 0.0684	0.0001	0.3084 ± 0.0444	0.0024
AngII – no bolus	0.5402 ± 0.0491 ^a	0.0029	0.4538 ± 0.0613 ^a	0.0850
AngII + hydralazine	0.6698 ± 0.0702 ^a	0.3272	0.6440 ± 0.0715 ^a	0.3896

Recognition indices of mice calculated from times spent exploring novel and original object in a novel object recognition memory task with 5 min or 24 h delay intervals. *n* = 10 per group; ^a*p* ≤ 0.05 compared to Angiotensin II (AngII). Values are expressed as mean ± SEM.

inability to discriminate between familiar and novel objects in both memory tasks, suggesting that the observed effects are primarily mediated by chronically elevated BP. Similarly, mice with developing hypertension (2 weeks post pump implantation, BP_{sys} ~ 120 mmHg; see Table 1: AngII 2 weeks) revealed similar recognition indices as we observed in control mice (Table 2: *p* = 0.4027 for 5 min delay and *p* = 0.9706 for 24 h delay).

Hypertension induces structural alterations in the brain

We utilized MRI and standard histological approaches to determine structural changes in the brain resulting from chronically elevated BP. As shown in Figure 2, AngII mice exhibited a larger total ventricle volume (Fig. 2a) and marked hippocampal atrophy (Fig. 2b) compared to saline controls. BP lowering therapy with hydralazine protected from both enlargement of ventricles and hippocampal atrophy. Although our mouse model lacked overt histological white matter lesions typically seen in human cSVD, DTI revealed significant white matter alterations in AngII mice. Deterioration of the white matter structures leads to loss of fiber orientation causing differences in water diffusivity, which can be evaluated by analyzing fractional anisotropy. Here, we analyzed fractional anisotropy in three major white matter regions (corpus callosum, internal capsula, and fimbria) and found it markedly lower in AngII mice compared to normotensive controls (Fig. 2c). Gray matter regions (cortex, thalamus, and hippocampus) showed no significant difference between normotensive and hypertensive mice (Figure S2). Furthermore, luxol blue staining of coronal brain sections indicated compromised integrity of myelin in the corpus callosum of hypertensive mice compared to normotensive controls (Figure S3).

BDNF, an important regulator of white matter integrity (Kiprianova *et al.* 1999; Bekinschtein *et al.* 2008; Blurton-Jones *et al.* 2009), was also negatively affected by chronic BP elevation: hypertension associated to lower BDNF expression in the corpus callosum compared to normotensive controls and mice preventatively treated with hydralazine (Fig. 2di–iii). Quantification revealed a markedly lower BDNF expression when normalized to NeuN+ cell count in

hypertensive mice compared to normotensive controls and hydralazine-treated mice, respectively (see Table S3: 4.47 ± 0.13 vs. 5.74 ± 0.23, *p* = 0.0012 and 4.47 ± 0.13 vs. 5.33 ± 0.25, *p* = 0.0168).

Hypertension distresses blood–brain barrier integrity and promotes neuroinflammation

Brain MRI analyses comprising a T2*-weighted sequence that visualizes vascular alterations, including microbleedings and hemorrhages, revealed differences between normotensive and hypertensive mice in week four of hypertension. Besides sporadic microbleedings identified histologically by hematoxylin and eosin stain (illustrated in Fig. 3b: representative images of coronal brain sections of hypertensive mice showing red blood cells in a distinguishable red-orange stain under hematoxylin and eosin), a significant larger area with overall hypointense pixels was revealed with the MRI approach, suggesting alterations in the cerebral vasculature during hypertension (Fig. 3a). In agreement with a previous study (Wakisaka *et al.* 2010), only hypertensive mice that received additional AngII bolus injections developed this phenotype (Figure S4).

In order to verify hypertension-mediated microanatomic alteration in the cerebral microvasculature, we characterized blood–brain barrier (BBB) integrity using an exogenous tracer (FITC–dextran 70 kDa). Although overt extravasation of FITC–dextran into the brain parenchyma was not detected, hypertensive mice showed a marked accumulation of FITC–dextran in the vessel walls of cerebral arteries compared to normotensive mice and mice treated with hydralazine (Fig. 3c). Interestingly, AngII mice revealed increased vascular accumulation of FITC-labeled dextran compared to mice from the AngII-no bolus group (Figure S5) supporting the MRI-based findings. Similarly, immune staining of albumin in coronal brain sections exposed BBB leakage only in AngII mice (Figure S6).

On the molecular level, chronically elevated BP affected crucial determinant of vascular integrity. Cerebral arteries isolated from AngII mice revealed significantly lower protein expression of vascular endothelial cadherin compared to vessels isolated from normotensive control or hydralazine-

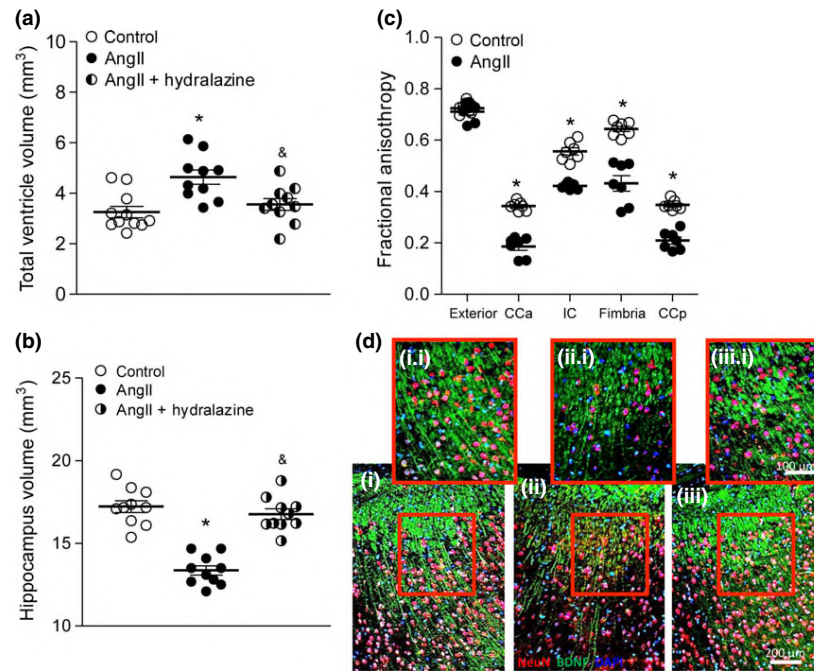


Fig. 2 Hypertension induces structural changes in the brain. (a) Total ventricle volume is enlarged in mice with chronic hypertension compared to normotensive controls and hydralazine-treated mice ($n = 10$ per group). (b) Chronic hypertension associates to hippocampal atrophy as evident by a reduced hippocampal volume compared to normotensive control mice and hydralazine-treated mice ($n = 10$ per group). (c) White matter integrity of prominent white matter regions (CCa, CCp – corpus callosum, IC – internal capsula, and fimbria) is compromised in hypertensive mice compared to normotensive controls

as evident by a reduced fractional anisotropy calculated from a diffusion tensor imaging approach ($n = 7$ per group). (d) Cerebral tissue sections showing immune staining for BDNF and NeuN in the corpus callosum of (i) normotensive controls, (ii) hypertensive mice, and (iii) hydralazine-treated mice ($n = 5$ per group). In (a and b) $*p \leq 0.05$ relative to control and $\&p \leq 0.05$ relative to AngII for multiple, unpaired comparisons; and in (c) $*p \leq 0.05$ relative to control for single, unpaired comparisons.

treated mice (Fig. 3d). Furthermore, the critical tight junction protein occludin was negatively affected by hypertension as evident by a markedly lower protein expression in cerebral arteries obtained from AngII mice compared to vessels obtained from normotensive control or hydralazine-treated mice (Fig. 3e).

Elevated cerebral artery smooth muscle actin expression evident of hypertrophic artery remodeling (Fig. 4ai–iv and c) and apparent reactive gliosis of glial fibrillary acidic protein-positive astrocytes surrounding cerebral vessels (Fig. 4ai,ii and b) indicate a critical impairment of cerebrovascular structure and neurovascular unit integrity in AngII mice. A significantly lower beta-type platelet-derived growth factor receptor expression in the brain of hypertensive mice compared to their normotensive controls indicates pericyte loss in arterioles and capillaries (Figure S8b and c). Together, these alterations might contribute to alterations in regional cerebral blood flow we observed in AngII mice (107.5 ± 11.1 mL/min/100 g vs. 147.1 ± 12.6 mL/min/100 g in striatum; $p = 0.036$; $n = 8$ and 144.7 ± 10.1 mL/min/100 g vs. 115.5 ± 3.8 mL/min/100 g in somatosensory

and motor cortex; $p = 0.045$; $n = 8$). Furthermore, hypertension associated to an up-regulation of the endothelial activation marker von Willebrand factor (vWF) (Fig. 4av,vi) and elevated mRNA expression levels of the cerebral artery adhesion molecules, vascular cell adhesion molecule-1, P-selectin, and E-selectin (Table S4) in our mouse model. These effects were accompanied by a marked accumulation of lymphocytes at the cerebral artery wall (Fig. 4av,vi), which might contribute to the increased wall thickness we observed in cerebral arteries of hypertensive mice (Fig. 4avii,viii and d).

Furthermore, hypertension induced microglial activation characterized by a reduction of ramifications (Fig. 5a) and an enlarged cell body (Fig. 5b). At the same time, cerebral mRNA expression of the pro-inflammatory cytokine TNF α , typically released by activated microglia, was up-regulated during hypertension (Fig. 5c).

Albeit having been conferred substantial pro-inflammatory effects, chronic AngII treatment failed to up-regulate mRNA expression of endothelial activation marker (vascular cell adhesion molecule-1, P-selectin and E-selectin) in the

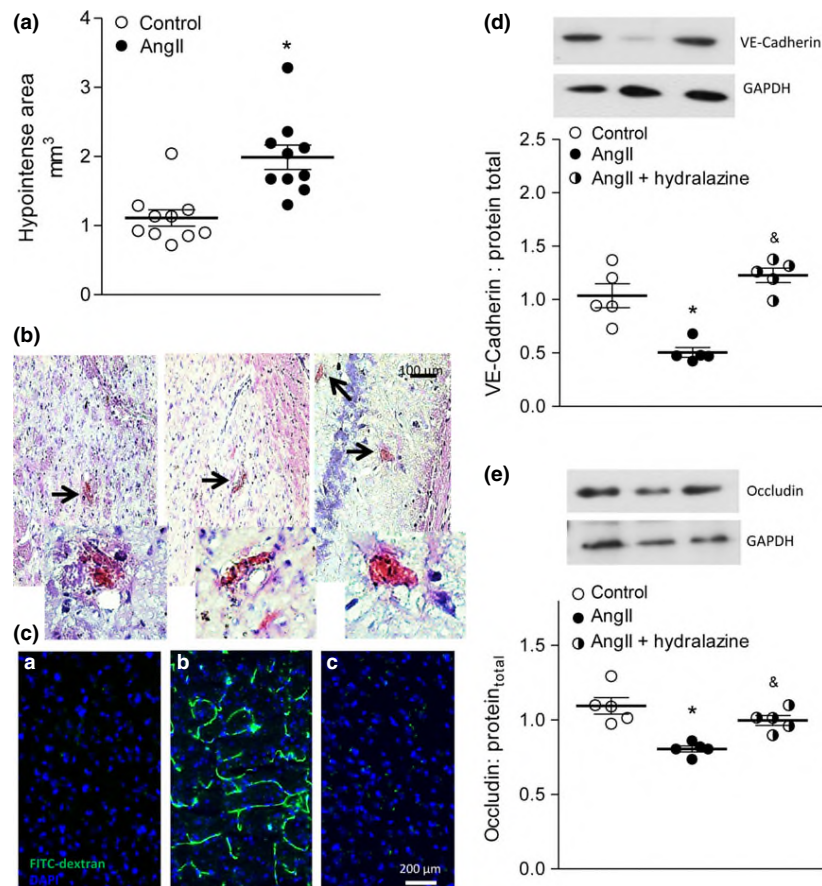


Fig. 3 Hypertension impairs blood–brain barrier integrity. (a) Algorithmic analysis of T2*-weighted magnetic resonance imaging revealed a significant increase in overall hypointense pixels in hypertensive mice ($n = 10$ per group). (b) Representative images showing (i) striatum, (ii) cortex, and (iii) hippocampus regions from hypertensive mice with sporadic microbleedings stained with hematoxylin and eosin. Red blood cells stain a distinguishable red-orange. (c) Representative images showing a cortical brain area from (i) normotensive, (ii) hypertensive mice, and (iii) hyalazine-treated mice. Green

fluorescence results from FITC–dextran (70 kDa) accumulation in the cerebral vasculature. (d) Vascular endothelial (VE) cadherin protein expression in cerebral arteries isolated from normotensive, hypertensive, and hyalazine-treated mice ($n = 5$ per group). (e) Total occludin protein expression in cerebral arteries isolated from normotensive, hypertensive, and hyalazine-treated mice ($n = 5$ per group). In (a) $*p \leq 0.05$ relative to control for single, unpaired comparisons; and in (d and e) $*p \leq 0.05$ relative to control, and $\&p \leq 0.05$ relative to AngII for multiple, unpaired comparisons.

presence of hyalazine (Table S4). Concomitant hyalazine treatment furthermore protected from hypertension-induced alterations of cerebrovascular structure (Figure S9). At the same time, preventative hyalazine treatment abolished microglia activation (Fig. 5a and b) and the augmentation of cerebral TNF α mRNA expression (Fig. 5c).

Discussion

In the present study, we characterize the consequences of chronically elevated BP on brain structure and function using a murine model of AngII-induced hypertension. Our data demonstrate that simultaneous treatment with AngII and the nitric oxide synthases inhibitor L-NAME induces profound hypertension that associates to cerebral alterations

reminiscent of early-onset cSVD and vascular cognitive impairment when combined with additional AngII bolus injections. Preventative application of a BP-lowering substance suggests that the above-described complications are rather attributable to chronically elevated BP than to direct effects of AngII itself. Our data support the suitability of this particular model as an animal model for early-onset cSVD and hence, vascular cognitive impairment, pathologies commonly preceding VaD.

The herein described model was established by modifying a hypertension protocol used for the induction of spontaneous intracerebral hemorrhages in mice (Wakisaka *et al.* 2010). Our findings confirm the development of microbleedings when mice are subjected to additional AngII bolus injections. However, by reducing duration and frequency of

Fig. 4 Hypertension negatively affects structure of cerebral arteries. (a) Representative images of coronal brain sections showing cerebral vessels stained with alpha-smooth muscle actin (α -SMA) in green and glial fibrillary acidic protein (GFAP) in red of (i) normotensive and (ii) hypertensive mice. Coronal sections of isolated cerebral arteries showing α -SMA expression in green in (iii) normotensive and (iv) hypertensive mice, the expression of vWF (green) and the accumulation of CD3 + T cells (red) at the cerebral artery wall in (v) normotensive and (vi) hypertensive mice. Coronal artery sections showing hematoxylin and eosin (H&E)-stained cerebral arteries from (vii) normotensive and (viii) hypertensive mice. (b) Cerebral GFAP protein expression ($n = 6$ per group). (c) Cerebral artery α -SMA mRNA expression ($n = 5$ per group). (d) Cerebral artery wall thickness obtained from H&E stained cerebral vessels ($n = 5$ per group). In (b–d) $*p \leq 0.05$ relative to control for single, unpaired comparisons.

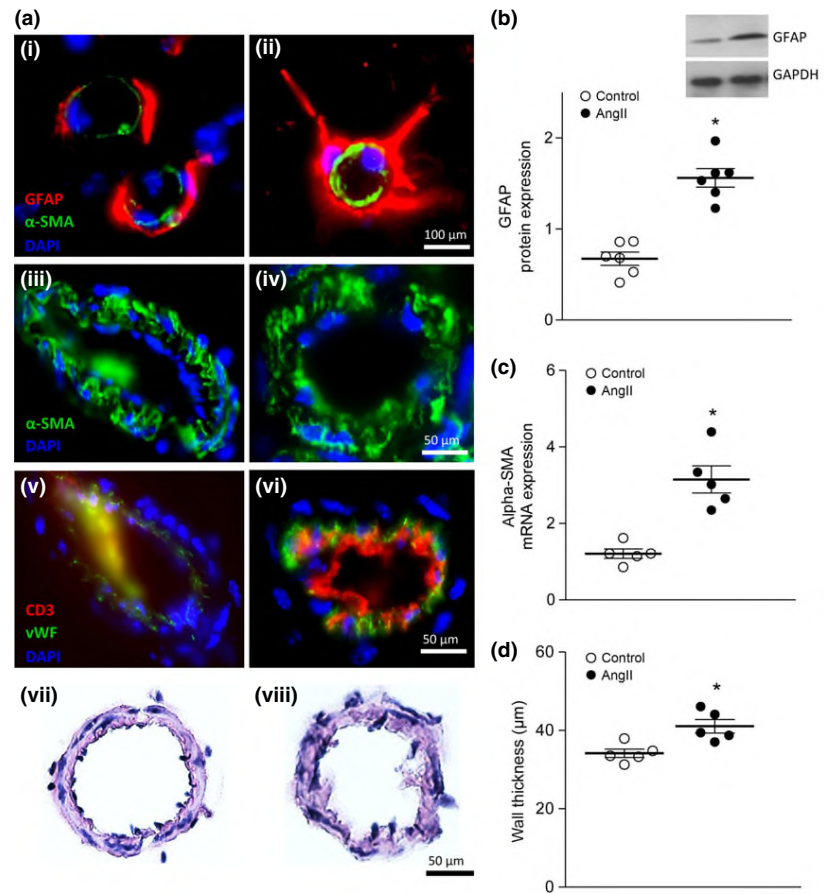
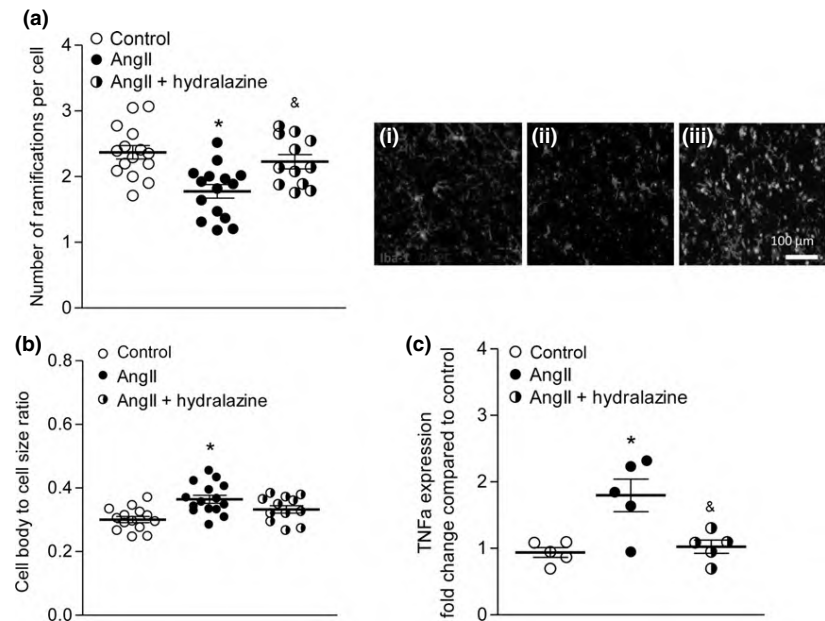


Fig. 5 Hypertension is accompanied by increased cerebral TNF α levels and activated microglia. (a) Brain tissue sections show evidence of microglial activation with microglia exhibiting visibly enlarged cytoplasm and reduced, thickened processes in (ii) hypertensive mice compared to (i) normotensive controls and (iii) hydralazine-treated mice. The number of dendrites per cell ($n = 5$ per group) and (b) the cell body-to-cell size ratios were calculated using a standardized macro in Image J in three different brain regions (cortex, hippocampus and striatum; $n = 5$ per group). (c) TNF α mRNA expression levels in brain tissue of normotensive, hypertensive and hydralazine-treated mice ($n = 5$ per group). In (a–c) $*p \leq 0.05$ relative to control, and $\&p \leq 0.05$ relative to AngII for multiple, unpaired comparisons.



AngII bolus injections and, most importantly, by using markedly younger animals, we develop a murine model of AngII-induced hypertension that resembles signs of a

subacute form of cSVD. Unlike Wakisaka *et al.* (2010) who describe the occurrence of spontaneous intracerebral hemorrhage and stroke signs as a result of additional AngII

bolus injections, we present a model characterized by cerebrovascular alterations associated with a mild form of cognitive impairment seemingly relevant for studying processes involved in the pathogenesis of cSVD and associated cognitive impairment.

Similar to SHR (Hainsworth and Markus 2008; Kaiser *et al.* 2014; Lopez-Gil *et al.* 2014), our mouse model of hypertension resembles morphological key features of human cSVD including hypertrophy of the cerebral vessel wall, structural impairment of the neurovascular unit, ventricular enlargement, and hippocampus atrophy. Additionally, we observe sporadic microscopic infarcts and microbleedings that have only been described in hypertensive mice and SHRSP with advanced age (Wakisaka *et al.* 2010; Schreiber *et al.* 2013; Toth *et al.* 2015), but that generally are associated with cognitive dysfunction accompanying vascular pathologies, such as leukoariosis, lacunar infarcts, large infarcts, as well as Alzheimer's disease (Greenberg *et al.* 2009; Smith 2012; Braun and Schreiber 2013; Yamashiro *et al.* 2014). Unlike aged SHR and SHRSP, our model lacks the obvious white matter lesions that are thought to evolve from a combination of demyelination, lacunar infarcts, and axonal loss (Hajjar *et al.* 2011; de Groot *et al.* 2013; van Uden *et al.* 2014). This obvious caveat certainly limits its use as a model of manifested cSVD when comparing it to the human phenotype. However, our model accords with cerebral alterations reminiscent of early-onset cSVD and vascular cognitive impairment and therefore, appears to be a suitable model to study the development of cSVD and contributing mechanisms. The lack of apparent white matter lesions might be resultant from the duration of AngII treatment in our experimental protocol. Compared to most studies performed in hypertensive mice or rats (Wakisaka *et al.* 2010; Kaiser *et al.* 2014; Toth *et al.* 2015), we induce hypertension in young mice for only 4 weeks, which might be too short to produce white matter lesions visible on MRI. However, a significant reduction in white matter density was detected using a DTI approach, which confirms results obtained in a SHR model (Lopez-Gil *et al.* 2014). Additionally, we find BDNF expression that has been conferred critical function in white matter maintenance in mice and men (Kennedy *et al.* 2009) to be less pronounced in important white matter structures of hypertensive mice compared to their respective normotensive controls.

BDNF expression has been furthermore described to play a critical role in hippocampal long-term potentiation and consequently, learning and memory, and has furthermore been attributed a protective effect for synaptic transmission and cognitive functions (Kiprianova *et al.* 1999; Bekinshtein *et al.* 2008; Blurton-Jones *et al.* 2009). It is therefore not surprising that in our mouse model, reduced hippocampal BDNF expression is accompanied by impaired cognitive functioning. Most importantly, albeit revealing a significantly lower mobility compared to normotensive controls that does

not seem to be resultant from locomotor deficits or impairment of visual perception, hypertensive mice do not show signs of increased anxiety, a common criticism in respect to cognitive deficits seen in the SHRSP model (Jiwa *et al.* 2010). Besides compromised hippocampal-dependent memory, hypertensive mice also reveal deficits in rhino-cortical memory traces, which may be attributable to cortical structural changes like for instance, alterations in number and morphology of dendritic spines, white matter alterations, or cerebral hypoperfusion because of an impaired blood flow regulation in small vessels as described for models of cardiovascular disease that comprise symptoms of cognitive decline (Markus *et al.* 2000, 2005; Vogels *et al.* 2007; Meissner *et al.* 2015).

Particularly, the cerebral microcirculation can be negatively affected by hypertension promoting the development of white matter lesions (Nation *et al.* 2015), since predominantly the terminal white matter arterioles (> 100 μm in diameter) are susceptible targets for pressure-induced structural alterations (Thore *et al.* 2007). Although we only used posterior cerebral arteries (120–150 μm in diameter) to investigate structural alterations in the cerebral vasculature, we confirm that chronically increased BP induces hypertrophic artery remodeling. However, the lower beta-type platelet-derived growth factor receptor expression in the brain of hypertensive mice suggests possible negative effects on arterioles and capillaries. Here, hypertension-induced pericyte loss could contribute to vessel rarefaction (Suzuki *et al.* 2003; Paiardi *et al.* 2009) that ultimately affects regional cerebral blood flow with deleterious consequences for, e.g., white matter integrity (Jiwa *et al.* 2010; Joutel *et al.* 2010). Besides the observed structural alterations of cerebral arteries, an L-NAME-mediated inhibition of endothelial nitric oxide synthases activity may as well impair vascular function and hence, the regulation of vascular tone and adequate tissue perfusion (Luscher 1990; Schiffrin *et al.* 2000). Moreover, our herein presented data align with studies showing the elevation of adhesion molecules, leukocyte rolling along cerebral vessels, T-cell infiltration, and accumulation in perivascular spaces during hypertension and suggest a causative link between vascular inflammation and structural alterations (Hainsworth and Markus 2008; van Hooren *et al.* 2014; Kaiser *et al.* 2014; Uiterwijk *et al.* 2015). Probably the major criticism of AngII hypertension model is due to the existence of non-pressor effects mediated by AngII. By showing that preventing AngII-induced BP elevation protects from cerebral artery inflammation and associated structural alterations, our data suggest that the observed brain effects are mainly due to the hypertensive action of AngII rather than to non-pressor effects of this drug. Nonetheless, further studies using other anti-hypertensive therapies are required to validate the herein reported effects.

Cerebrovascular leakage emanating from pro-inflammatory processes occur during neurodegenerative diseases

(Schreiber *et al.* 2013), but were also associated with cSVD, lacunar infarcts, and with hypertension (Henning *et al.* 2010; Giwa *et al.* 2012; Jalal *et al.* 2012; Hainsworth *et al.* 2015; Uiterwijk *et al.* 2015; Wiseman *et al.* 2015). However, it remains elusive whether BBB dysfunction is the *primary cause* to changes in the cerebral microvasculature since to date, studies only reported an increased BBB permeability at times of clinically evident cSVD (Farrall and Wardlaw 2009; Wardlaw *et al.* 2009). Nevertheless, increasing numbers of activated circulating immune cell, endothelial activation, and the presence of activated microglia in the central nervous system of hypertensive individuals suggest a link between cardiovascular risk factors and BBB impairment (Marvar *et al.* 2011; Kaiser *et al.* 2014; Meissner *et al.* 2015). In the herein presented mouse model of hypertension, we observe a marked activation of microglia associated to an increase in cerebral levels of the pro-inflammatory cytokine TNF α along with signs of BBB leakage, endothelial activation, and enhanced immune cell accumulation at the cerebral vessel wall that would allow for studies concerning the primary cause to changes in the cerebral microcirculation during hypertension. Moreover, this model provides potential to study hypertension-mediated neuroinflammation and particularly, cerebral TNF α augmentation, which not only occurs after acute brain injury or ischemia, but also during neurodegenerative diseases and after systemic inflammatory challenge with devastating consequences for neuronal structures and hence, cognitive function (Smith *et al.* 2012; Yang *et al.* 2012; Zhou *et al.* 2013; Meissner *et al.* 2015).

Conclusions and perspective

Although hypertension is widely accepted as a major modifiable risk factor for the development of VaD and preceding vascular cognitive impairment, experimental approaches tackling the mechanisms underlying VaD mostly utilize animal models of altered blood flow, cerebral amyloid angiopathy, multiple infarction, or genetic models. Purely risk factor-based models only include a small number of diabetes or aging-related mouse models and the SHR/SHRSP model. With the herein presented model of hypertension-mediated cognitive impairment, we provide a murine model that resembles key features of early-onset cSVD including arteriopathy, BBB impairment, incipient signs of white matter alterations, neuroinflammation, and with a neuropsychological profile typical for cSVD. Given the diversity of pathologies underlying VaD, there is no optimal model to study the molecular mechanisms leading to cognitive decline. However, a mouse model with metabolic similarity to humans, such as hypertension, seems appropriate to advance the proper understanding of disease pathogenesis, the search for effective treatment strategies, and the identification of potential biomarkers for VaD, so that the incidence of this

disorder might eventually be reduced. The complexity of processes underlying the pathogenic effects of hypertension on the microvasculature in the brain however, certainly requires a more specific evaluation of mechanisms contributing to cerebrovascular alterations underlying cognitive decline. Specifically, the relative importance of oxidative stress and the type of BBB impairment causal to neuroinflammatory processes represent vital questions future studies need to urgently address.

Acknowledgments and conflict of interest disclosure

The authors are grateful to Dr. Lluïsa Camon, Ms. Francisca Ruiz, Ms. Maike Hoppen, and Ms. Birgit Geng for technical help. We gratefully acknowledge the following funding support research grant from the Spanish Ministry of Economy (MICINN SAF2014-56279), a Marie Curie Action of the 7th Framework Program of the European Commission (AM; 2013_229673), a stipend for returning scientists granted from the German Academic Exchange Service (AM; PKZ2015_91606607), and the Else Kröner Fresenius Stiftung (JM; 2014_EKES.16). The authors have no conflict of interest to declare.

All experiments were conducted in compliance with the ARRIVE guidelines.

Supporting information

Additional Supporting Information may be found online in the supporting information tab for this article:

Appendix S1. Supplementary materials and methods.

Figure S1. Behavioral assessment of hypertensive mice compared to normotensive controls.

Figure S2. Diffusion-tensor imaging (DTI) measures obtained in week four of hypertension.

Figure S3. Luxol blue-stained myelin in coronal brain sections of normotensive and hypertensive mice.

Figure S4. Cerebrovascular alterations and potential microbleedings obtained using MRI with a T2*-weighted sequence.

Figure S5. FITC-dextran quantification in cerebral arteries of normotensive and hypertensive mice.

Figure S6. Quantification of BBB leakage to albumin in normotensive, hypertensive, and hydralazine-treated mice.

Figure S7. Representative WB experiments.

Figure S8. GFAP and PDGFR-beta mRNA expression of normotensive and hypertensive mice.

Figure S9. Analysis of vessel wall structure and integrity of the neurovascular unit of cerebral arteries obtained from AngII mice and mice preventatively treated with hydralazine.

Table S1. Overview experimental protocol and timeline.

Table S2. Behavioral parameters obtained during an open-field approach and during a light-dark exploration task.

Table S3. Quantification of immune-stained NeuN+ and BDNF+ brain regions from normotensive, hypertensive, and hydralazine-treated mice.

Table S4. Comparison of inflammatory marker in hypertensive versus normotensive mice.

References

- Ayata C. (2010) CADASIL: experimental insights from animal models. *Stroke* **41**, S129–S134.
- Baker K. B. and Kim J. J. (2002) Effects of stress and hippocampal NMDA receptor antagonism on recognition memory in rats. *Learn. Mem.* **9**, 58–65.
- Bekinschtein P., Cammarota M., Katche C., Slipczuk L., Rossato J. I., Goldin A., Izquierdo I. and Medina J. H. (2008) BDNF is essential to promote persistence of long-term memory storage. *Proc. Natl Acad. Sci. USA* **105**, 2711–2716.
- Blurton-Jones M., Kitazawa M., Martinez-Coria H. *et al.* (2009) Neural stem cells improve cognition via BDNF in a transgenic model of Alzheimer disease. *Proc. Natl Acad. Sci. USA* **106**, 13594–13599.
- Braun H. and Schreiber S. (2013) Microbleeds in cerebral small vessel disease. *Lancet Neurol.* **12**, 735–736.
- Brown W. R., Moody D. M., Thore C. R., Challa V. R. and Anstrom J. A. (2007) Vascular dementia in leukoaraiosis may be a consequence of capillary loss not only in the lesions, but in normal-appearing white matter and cortex as well. *J. Neurol. Sci.* **257**, 62–66.
- Chan S. L., Sweet J. G. and Cipolla M. J. (2013) Treatment for cerebral small vessel disease: effect of relaxin on the function and structure of cerebral parenchymal arterioles during hypertension. *FASEB J.* **27**, 3917–3927.
- Chang-Quan H., Hui W., Chao-Min W., Zheng-Rong W., Jun-Wen G., Yong-Hong L., Yan-You L. and Qing-Xiu L. (2011) The association of antihypertensive medication use with risk of cognitive decline and dementia: a meta-analysis of longitudinal studies. *Int. J. Clin. Pract.* **65**, 1295–1305.
- Chui H. (2001) Dementia due to subcortical ischemic vascular disease. *Clin Cornerstone* **3**, 40–51.
- Farrall A. J. and Wardlaw J. M. (2009) Blood-brain barrier: ageing and microvascular disease—systematic review and meta-analysis. *Neurobiol. Aging* **30**, 337–352.
- Francis B. M., Kim J., Barakat M. E. *et al.* (2012) Object recognition memory and BDNF expression are reduced in young TgCRND8 mice. *Neurobiol. Aging* **33**, 555–563.
- Faul F., Erdfelder E., Lang A. G. and Buchner A. (2007) G*Power 3: a flexible statistical power analysis program for the social, behavioral, and biomedical sciences. *Behav. Res. Methods* **39**, 175–191.
- Giwa M. O., Williams J., Elderfield K., Jiwa N. S., Bridges L. R., Kalaria R. N., Markus H. S., Esiri M. M. and Hainsworth A. H. (2012) Neuropathologic evidence of endothelial changes in cerebral small vessel disease. *Neurology* **78**, 167–174.
- Gooch J. and Wilcock D. M. (2016) Animal models of vascular cognitive impairment and dementia (VCID). *Cell. Mol. Neurobiol.* **36**, 233–239.
- Greenberg S. M., Vernooij M. W., Cordonnier C. *et al.* (2009) Cerebral microbleeds: a guide to detection and interpretation. *Lancet Neurol.* **8**, 165–174.
- de Groot M., Verhaaren B. F., de Boer R., Klein S., Hofman A., van der Lugt A., Ikram M. A., Niessen W. J. and Vernooij M. W. (2013) Changes in normal-appearing white matter precede development of white matter lesions. *Stroke* **44**, 1037–1042.
- Hachinski V. (2006) Commentary on “Vascular cognitive impairment: today and tomorrow”. Vascular cognitive impairment: yesterday, today, and tomorrow. *Alzheimers Dement.* **2**, 198–199.
- Hainsworth A. H. and Markus H. S. (2008) Do *in vivo* experimental models reflect human cerebral small vessel disease? A systematic review. *J. Cereb. Blood Flow Metab.* **28**, 1877–1891.
- Hainsworth A. H., Oommen A. T. and Bridges L. R. (2015) Endothelial cells and human cerebral small vessel disease. *Brain Pathol.* **25**, 44–50.
- Hajjar I., Quach L., Yang F., Chaves P. H., Newman A. B., Mukamal K., Longstreth W., Jr, Inzitari M. and Lipsitz L. A. (2011) Hypertension, white matter hyperintensities, and concurrent impairments in mobility, cognition, and mood: the Cardiovascular Health Study. *Circulation* **123**, 858–865.
- Hammond R. S., Tull L. E. and Stackman R. W. (2004) On the delay-dependent involvement of the hippocampus in object recognition memory. *Neurobiol. Learn. Mem.* **82**, 26–34.
- Helman A. M. and Murphy M. P. (2016) Vascular cognitive impairment: modeling a critical neurologic disease *in vitro* and *in vivo*. *Biochim. Biophys. Acta* **1862**, 975–982.
- Henning E. C., Warach S. and Spatz M. (2010) Hypertension-induced vascular remodeling contributes to reduced cerebral perfusion and the development of spontaneous stroke in aged SHRSP rats. *J. Cereb. Blood Flow Metab.* **30**, 827–836.
- van Hooren K. W., Spijkers L. J., van Breevoort D., Fernandez-Borja M., Bierings R., van Buul J. D., Alewijnse A. E., Peters S. L. and Voorberg J. (2014) Sphingosine-1-phosphate receptor 3 mediates sphingosine-1-phosphate induced release of weibel-palade bodies from endothelial cells. *PLoS ONE* **9**, e91346.
- Huijts M., Duits A., van Oostenbrugge R. J., Kroon A. A., de Leeuw P. W. and Staals J. (2013) Accumulation of MRI markers of cerebral small vessel disease is associated with decreased cognitive function. A Study in First-Ever Lacunar Stroke and Hypertensive Patients. *Front. Aging Neurosci.* **5**, 72.
- Huijts M., Duits A., Staals J., Kroon A. A., de Leeuw P. W. and van Oostenbrugge R. J. (2014) Basal ganglia enlarged perivascular spaces are linked to cognitive function in patients with cerebral small vessel disease. *Curr. Neurovasc. Res.* **11**, 136–141.
- Iadecola C. (2014) Hypertension and dementia. *Hypertension* **64**, 3–5.
- Imamine R., Kawamura T., Umemura T. *et al.* (2011) Does cerebral small vessel disease predict future decline of cognitive function in elderly people with type 2 diabetes? *Diabetes Res. Clin. Pract.* **94**, 91–99.
- Jalal F. Y., Yang Y., Thompson J., Lopez A. C. and Rosenberg G. A. (2012) Myelin loss associated with neuroinflammation in hypertensive rats. *Stroke* **43**, 1115–1122.
- Jiwa N. S., Garrard P. and Hainsworth A. H. (2010) Experimental models of vascular dementia and vascular cognitive impairment: a systematic review. *J. Neurochem.* **115**, 814–828.
- Joutel A., Monet-Lepretre M., Gosele C. *et al.* (2010) Cerebrovascular dysfunction and microcirculation rarefaction precede white matter lesions in a mouse genetic model of cerebral ischemic small vessel disease. *J. Clin. Investig.* **120**, 433–445.
- Kaiser D., Weise G., Moller K. *et al.* (2014) Spontaneous white matter damage, cognitive decline and neuroinflammation in middle-aged hypertensive rats: an animal model of early-stage cerebral small vessel disease. *Acta Neuropathol. Commun.* **2**, 169.
- Kennedy K. M., Rodrigue K. M., Land S. J. and Raz N. (2009) BDNF Val66Met polymorphism influences age differences in microstructure of the Corpus Callosum. *Front. Hum. Neurosci.* **3**, 19.
- Kiprianova I., Sandkuhler J., Schwab S., Hoyer S. and Spranger M. (1999) Brain-derived neurotrophic factor improves long-term potentiation and cognitive functions after transient forebrain ischemia in the rat. *Exp. Neurol.* **159**, 511–519.
- Lopez-Gil X., Amat-Roldan I., Tudela R., Castane A., Prats-Galino A., Planas A. M., Farr T. D. and Soria G. (2014) DWI and complex brain network analysis predicts vascular cognitive impairment in spontaneous hypertensive rats undergoing executive function tests. *Front. Aging Neurosci.* **6**, 167.
- Luscher T. F. (1990) Imbalance of endothelium-derived relaxing and contracting factors. A new concept in hypertension? *Am. J. Hypertens.* **3**, 317–330.

- Markus H. S., Lythgoe D. J., Ostegaard L., O'Sullivan M. and Williams S. C. (2000) Reduced cerebral blood flow in white matter in ischaemic leukoaraiosis demonstrated using quantitative exogenous contrast based perfusion MRI. *J. Neurol. Neurosurg. Psychiatry* **69**, 48–53.
- Markus H. S., Hunt B., Palmer K., Enzinger C., Schmidt H. and Schmidt R. (2005) Markers of endothelial and hemostatic activation and progression of cerebral white matter hyperintensities: longitudinal results of the Austrian Stroke Prevention Study. *Stroke* **36**, 1410–1414.
- Marvar P. J., Lob H., Vinh A., Zarreen F. and Harrison D. G. (2011) The central nervous system and inflammation in hypertension. *Curr. Opin. Pharmacol.* **11**, 156–161.
- Meissner A. (2016) Hypertension and the brain: a risk factor for more than heart disease. *Cerebrovasc. Dis.* **42**, 255–262.
- Meissner A., Visanji N. P., Momen M. A., Feng R., Francis B. M., Bolz S. S. and Hazrati L. N. (2015) Tumor necrosis factor- α underlies loss of cortical dendritic spine density in a mouse model of congestive heart failure. *J. Am. Heart Assoc.* **4**.
- Mitnitski A., Skoog I., Song X., Waern M., Ostling S., Sundh V., Steen B. and Rockwood K. (2006) A vascular risk factor index in relation to mortality and incident dementia. *Eur. J. Neurol.* **13**, 514–521.
- Moorhouse P. and Rockwood K. (2008) Vascular cognitive impairment: current concepts and clinical developments. *Lancet Neurol.* **7**, 246–255.
- Nation D. A., Edmonds E. C., Bangen K. J. *et al.* (2015) Pulse pressure in relation to tau-mediated neurodegeneration, cerebral amyloidosis, and progression to dementia in very old adults. *JAMA Neurol.* **72**, 546–553.
- Paiardi S., Rodella L. F., De Ciuceis C. *et al.* (2009) Immunohistochemical evaluation of microvascular rarefaction in hypertensive humans and in spontaneously hypertensive rats. *Clin. Hemorheol. Micro.* **42**, 259–268.
- Rohn T. T. (2014) Is apolipoprotein E4 an important risk factor for vascular dementia? *Int. J. Clin. Exp. Pathol.* **7**, 3504–3511.
- Rohn T. T., Day R. J., Sheffield C. B., Rajic A. J. and Poon W. W. (2014) Apolipoprotein E pathology in vascular dementia. *Int. J. Clin. Exp. Pathol.* **7**, 938–947.
- Schiffirin E. L., Park J. B., Intengan H. D. and Touyz R. M. (2000) Correction of arterial structure and endothelial dysfunction in human essential hypertension by the angiotensin receptor antagonist losartan. *Circulation* **101**, 1653–1659.
- Schreiber S., Bueche C. Z., Garz C. and Braun H. (2013) Blood brain barrier breakdown as the starting point of cerebral small vessel disease? - New insights from a rat model. *Exp. Transl. Stroke Med.* **5**, 4.
- Smith C. D. (2012) Structural imaging in early pre-states of dementia. *Biochim. Biophys. Acta* **1822**, 317–324.
- Smith J. A., Das A., Ray S. K. and Banik N. L. (2012) Role of pro-inflammatory cytokines released from microglia in neurodegenerative diseases. *Brain Res. Bull.* **87**, 10–20.
- Suzuki K., Masawa N., Sakata N. and Takatama M. (2003) Pathologic evidence of microvascular rarefaction in the brain of renal hypertensive rats. *J. Stroke Cerebrovasc. Dis.* **12**, 8–16.
- Thore C. R., Anstrom J. A., Moody D. M., Challa V. R., Marion M. C. and Brown W. R. (2007) Morphometric analysis of arteriolar tortuosity in human cerebral white matter of preterm, young, and aged subjects. *J. Neuropathol. Exp. Neurol.* **66**, 337–345.
- de la Torre J. C. (2012) Cardiovascular risk factors promote brain hypoperfusion leading to cognitive decline and dementia. *Cardiovasc. Psychiatry Neurol.* **2012**, 367516.
- Toth P., Tarantini S., Springo Z. *et al.* (2015) Aging exacerbates hypertension-induced cerebral microhemorrhages in mice: role of resveratrol treatment in vasoprotection. *Aging Cell* **14**, 400–408.
- van Uden I. W., Tuladhar A. M., de Laat K. F., van Norden A. G., Norris D. G., van Dijk E. J., Tendolkar I. and de Leeuw F. E. (2014) White matter integrity and depressive symptoms in cerebral small vessel disease: the RUN DMC Study. *Am. J. Geriatr. Psychiatry* **23**, 525–535.
- Uiterwijk R., Huijts M., Staals J., Rouhl R. P., De Leeuw P. W., Kroon A. A. and Van Oostenbrugge R. J. (2015) Endothelial activation is associated with cognitive performance in patients with hypertension. *Am. J. Hypertens.* **29**, 464–469.
- Venkat P., Chopp M. and Chen J. (2015) Models and mechanisms of vascular dementia. *Exp. Neurol.* **272**, 97–108.
- Vogels R. L., Oosterman J. M., van Harten B., Gouw A. A., Schroeder-Tanka J. M., Scheltens P., van der Flier W. M. and Weinstein H. C. (2007) Neuroimaging and correlates of cognitive function among patients with heart failure. *Dement. Geriatr. Cogn. Disord.* **24**, 418–423.
- Wakisaka Y., Chu Y., Miller J. D., Rosenberg G. A. and Heistad D. D. (2010) Spontaneous intracerebral hemorrhage during acute and chronic hypertension in mice. *J. Cereb. Blood Flow Metab.* **30**, 56–69.
- Wardlaw J. M., Doubal F., Armitage P. *et al.* (2009) Lacunar stroke is associated with diffuse blood-brain barrier dysfunction. *Ann. Neurol.* **65**, 194–202.
- Wiseman S. J., Doubal F. N., Chappell F. M., Valdes-Hernandez M. C., Wang X., Rumley A., Lowe G. D., Dennis M. S. and Wardlaw J. M. (2015) Plasma biomarkers of inflammation, endothelial function and hemostasis in cerebral small vessel disease. *Cerebrovasc. Dis.* **40**, 157–164.
- Yamashiro K., Tanaka R., Okuma Y., Shimura H., Ueno Y., Miyamoto N., Urabe T. and Hattori N. (2014) Cerebral microbleeds are associated with worse cognitive function in the nondemented elderly with small vessel disease. *Cerebrovasc. Dis. Extra* **4**, 212–220.
- Yang J., Noyan-Ashraf M. H., Meissner A. *et al.* (2012) Proximal cerebral arteries develop myogenic responsiveness in heart failure via tumor necrosis factor- α -dependent activation of sphingosine-1-phosphate signaling. *Circulation* **126**, 196–206.
- Zhou W., Liesz A., Bauer H., Sommer C., Lahrmann B., Valous N., Grabe N. and Veltkamp R. (2013) Postischemic brain infiltration of leukocyte subpopulations differs among murine permanent and transient focal cerebral ischemia models. *Brain Pathol.* **23**, 34–44.